Available online at www.sciencedirect.com
ScienceDirect
Catalysis Today 123 (2007) 265–275
CATALYSIS TODAY
www.elsevier.com/locate/cattod

Oxidation and reforming reactions of CH_4 on a stepped Pt(5 5 7) single crystal

Robert M. Rioux [1], Anderson L. Marsh [2], J.S. Gaughan, G.A. Somorjai *

Department of Chemistry, University of California, Berkeley and Materials Sciences Division, Lawrence Berkeley National Laboratory, Berkeley, CA 94720, USA

Available online 28 March 2007

Abstract

The oxidation and reforming kinetics of methane by O_2, CO_2 and H_2O were studied on a stepped Pt(5 5 7) single crystal from 623 to 1050 K under methane rich conditions. The rate of carbon deposition was followed by ex-situ Auger electron spectroscopy under non-oxidative conditions. The apparent activation energy for methane decomposition was significantly lower than the apparent barriers measured for both total oxidation, CO_2 and H_2O reforming. Total oxidation of methane to CO_2 and H_2O followed by combined dry and steam reforming (combined combustion-reforming) led to CO production rates which were higher than direct CO_2 or H_2O reforming rates. The enhanced rates are most likely due to the ability of adsorbed oxygen to prevent carbon nucleation and/or scavenge carbon enabling the reforming reaction to turnover on a larger fraction of sites. Comparable amounts of carbon were found by Auger electron spectroscopy measurements after both direct dry or steam reforming, while combined oxidation-reforming had considerable less carbon. During direct dry or steam reforming, CO_2 and H_2O serve only to scavenge adsorbed atomic carbon, while in the presence of oxygen, carbon is removed by both combustion and reforming routes.

Keywords: Oxidation; Reforming; combined combustion-reforming; Methane; Oxygen; Pt single crystal; Steps

1. Introduction

The conversion of methane to oxygenates and higher carbon number alkanes/alkenes is vital to a sustainable energy future [1,2]. Current methods for direct conversion of methane (i.e. oxidative coupling [3,4]) suffer from low yield and therefore not suitable for industrial implementation. An intermediary step to direct conversion is the formation of syngas (CO and H_2) from methane [5]. Separate catalytic chemistry enables formation of higher alkanes/alkenes with Fe or Co based catalysts (Fischer Tropsch synthesis) and oxygenates from Cu based catalysts (methanol synthesis). Both steam ($CH_4 + H_2O \rightarrow CO + 3H_2$) and dry ($CH_4 + CO_2 \rightarrow 2CO + 2H_2$) reforming are standard methods for syngas production. Both reactions are highly endothermic and suffer from severe deactivation due to carbon deposition. Carbon dioxide reforming is the preferred method of syngas formation because the lower CO:H_2 ratio is ideal for Fischer Tropsch synthesis [6] and uses feedstocks which are inexpensive due to their large natural abundance. Industrially, steam reforming is the preferred method for syngas formation because Ni based catalysts optimized for steam reforming are less susceptible to catalyst deactivation by carbon deposition, although some industrial CH_4–CO_2 processes exist. Both chemistries suffer from poor thermodynamics requiring high temperatures to achieve reasonable conversions. Nickel is the catalyst of choice because of the high cost of noble metals such as Pt, yet Pt catalysts are more active than Ni catalysts on a per surface atom basis when rates are rigorously corrected for transport artifacts and equilibrium effects [7,8]. Pt catalysts are generally more resistant to deactivation by carbon deposition [9]. A rather complete review of carbon deposition during methanation and steam reforming on nickel is given in [10]. The ability to design low weight loading, highly active Pt reforming catalysts is still important due to the increased interest in the hydrogen economy and synthetic fuels.

* Corresponding author.
E-mail address: somorjai@berkeley.edu (G.A. Somorjai).
[1] Present address: Department of Chemistry and Chemical Biology, Harvard University, Cambridge, MA 02138, USA.
[2] Present address: Department of Chemistry, Lebanon Valley College, Annville, PA 17003, USA.

0920-5861/$ – see front matter © 2007 Elsevier B.V. All rights reserved.
doi:10.1016/j.cattod.2007.02.018

Another route to syngas formation through thermodynamically favorable chemistry, such as direct partial oxidation ($CH_4 + 1/2O_2 \rightarrow CO + 2H_2$, $\Delta H^\circ_{298\,K} = -8.5\,kcal\,mol^{-1}\,CH_4$) is potentially promising because of favorable yields and CO/H_2 ratio for further conversion. These reactions however suffer from competing thermodynamically more favorable reactions such as total combustion ($CH_4 + 2O_2 \rightarrow CO_2 + 2H_2O$). The exact pathway of partial oxidation is debated; direct oxidation of surface carbon to CO has been proposed in short contact time reactors [11,12], while an indirect mechanism—combined combustion followed by reforming has been postulated [13].

In this paper, we study two aspects of syngas formation using combined UHV-high pressure (HP) techniques; the non-oxidative decomposition of methane with sum frequency generation (SFG) surface vibrational spectroscopy and the reaction kinetics of both direct methane (steam and dry) reforming and combined combustion-reforming on a stepped Pt(5 5 7) single crystal surface. The kinetics of methane reforming is proportional to the amount of co-reactant (CO_2, H_2O, O_2) under fuel rich conditions. The rate of combined total combustion-reforming was a factor of ~1.5–2 higher than direct dry reforming reaction at similar conditions. Ex-situ Auger electron spectroscopy analysis of the single crystal surface after reaction suggested that it is most likely due to the removal of carbonaceous deposits by the oxygen from the surface. This unique pathway due to the presence of chemisorbed oxygen favored the removal of adsorbed carbon by oxidation to CO_2, thereby enabling unpoisoned active sites and CO_2 to reenter the catalytic cycle.

2. Experimental

2.1. Ultrahigh vacuum chamber and Pt(5 5 7) single crystal preparation

All experiments were conducted in an ultrahigh vacuum (UHV) chamber pumped by ion and turbomolecular pumps to a base pressure of 2×10^{-10} Torr. The chamber was equipped with a retarding field analyzer (Omicron SPECTALEED) for Auger electron spectroscopy (AES) and rearview low energy electron diffraction (LEED). AES spectra of the surface after reaction were collected at 1×10^{-8} Torr from ~100 to 550 eV, covering the range of major Pt peaks (158, 172, 220, and 239 eV), C (274 eV) and O (530 eV). The chamber was equipped with a mass spectrometer (Stanford Research Systems, 100 amu residual gas analyzer) to monitor the concentration of background gases. The Pt(5 5 7) single crystal could be heated to temperatures greater than 1200 K by resistive heating through Ni–Cr wires spotwelded to the side of the single crystal and cooled to temperatures of ~140 K using liquid nitrogen. The temperature was monitored by a chromel alumel type K thermocouple (Omega Engineering, Stamford, CT) spotwelded to the back side of the crystal.

A Pt(5 5 7) surface was prepared by cutting a platinum single crystal 9.5° relative to the (1 1 1) orientation. The stepped surface has six atom wide terraces of (1 1 1) orientation and single atom high steps of (1 0 0) orientation with step atoms constituting 1/6 of the total number of surface atoms [14]. The coordination number of the terrace atoms is nine, while the atoms constituting the step have only seven nearest neighbors [14]. The single crystal (0.8 cm^2) used in this study was highly polished by standard protocol, mounted on a sample manipulator with *x-y-z* motion and 360° rotation capabilities, and cleaned by standard procedures. The crystal surface was sputtered with two cycles of Ar^+ at 2×10^{-5} Torr followed by exposure to 5×10^{-7} Torr O_2 at 1125 K for 2 min followed by annealing in vacuum at 1135 K for 1 min. After annealing, the Pt(5 5 7) was slowly cooled (10 K min^{-1}) to 673 K, followed by quickly cooling to room temperature.

2.2. Catalytic reactions of CH_4 with O_2 or H_2O/CO_2 in UHV apparatus

All kinetic experiments were conducted in a 30 L bell jar or within a small (350 mL) high pressure reaction cell which was isolated from the main UHV chamber by a gate valve. The crystal could be transferred from the UHV chamber to the high pressure cell using a linear motion transfer arm. After crystal cleaning, the chamber pressure was allowed to reach $\sim 10^{-9}$ Torr before gases were introduced. Gases were introduced in the same order for each experiment. Oxygen (or carbon monoxide or water) was introduced, followed by methane, and then the chamber was backfilled with He to a total pressure of ~800 Torr. For all reactions, the bell jar or the high pressure cell operated as a recirculating batch reactor. The gases were mixed by a recirculation pump (Senior Flexonics Metal Bellows Model MB-21, Sharon, MA) at a nominal rate of ~1000 $cm^3\,min^{-1}$ for a 1/2 h before blank injections. Gas phase concentrations were monitored with a gas chromatograph (Hewlett Packard 5890) using a packed column (Supelco, 1/8 in. × 20 ft, 60/80 Carboxen-1000, Bellefonte, PA). Once methane and CO_2 or oxygen GC area counts stabilized, the crystal was quickly heated to the reaction temperature with minimal overshoot and reaction time commenced. H_2O and H_2 were not detectable in the current chromatographic set up preventing the determination of O_2 and H_2 mass balances. Turnover rates were calculated from the slope of the turnover number versus time plot. Turnover number is defined as the number of reacted or produced molecules per surface site. The number of surface sites was calculated assuming a site density of $\sim 1.4 \times 10^{15}$ atoms cm^{-2} and rates were normalized to the total density rather than the step site density ($\sim 10^{14}$ cm^{-2}).

2.3. Sum frequency generation (SFG) surface vibrational spectroscopy

The adsorption of carbon monoxide and the non-oxidative decomposition of CH_4 were followed with sum frequency generation (SFG) surface vibrational spectroscopy. The adsorption of CO on a clean Pt(5 5 7) surface has been studied [15,16] and this paper only comments on the influence of CO–CH_4 coadsorption on the CO SFG spectrum. The UHV chamber was equipped with a pair of CaF_2 windows to enable entry of a

visible (532 nm), tunable infrared beam (1800–4000 cm^{-1}) and exit of a sum frequency beam (400–450 nm). Infrared and visible laser beams were generated from a commercial Nd:YAG (Leopard Continuum, Santa Clara, CA) laser operated at 20 Hz with a 20 ps pulse duration and a pulse energy of 35 mJ at a fundamental frequency of 1064 nm. The resultant pulse was used to pump an optical parametric generation-amplification (OPG/OPA) (LaserVision, Bellevue, WA) system. The fundamental beam was split with one portion sent through a Potassium Titanium Oxide Phosphate (KTP) crystal to generate a 532 nm beam, which was further split with one portion serving as the visible beam for SFG while the other portion was sent through two counter rotating KTP crystals in the OPG/OPA to generate a near-IR beam (720–870 nm). This near IR beam was difference frequency mixed with a portion of the fundamental beam through counter rotating Potassium Titanyl Arsenate (KTA) crystals to produce a tunable mid-IR beam between 2000 and 4000 cm^{-1}. The energy at 2100 cm^{-1} is 200 μJ with a full width at half maximum (FWHM) of 8 cm^{-1}, while at 3000 cm^{-1}, the energy is 400 μJ and the FWHM is 10 cm^{-1} [17]. More details on the laser system can be found elsewhere [16–18].

In SFG, the visible and tunable infrared beams are spatially and temporally overlapped on the surface. The visible beam impinges the surface at 60° relative to the surface normal, while the infrared beam impinges 70° relative to the normal. Both input beams are p-polarized resulting in outgoing p-polarized SFG photons. As the tunable infrared beam is scanned across the infrared portion of the spectrum, a vibrational spectrum of adsorbates is obtained. The generated SFG photons are sent to a monochromator and the signal intensity of SFG photons is monitored by a photomultiplier tube (PMT) and integrated by a gated integrator. The theory of SFG at the solid–gas interface has been previously reviewed by others [19].

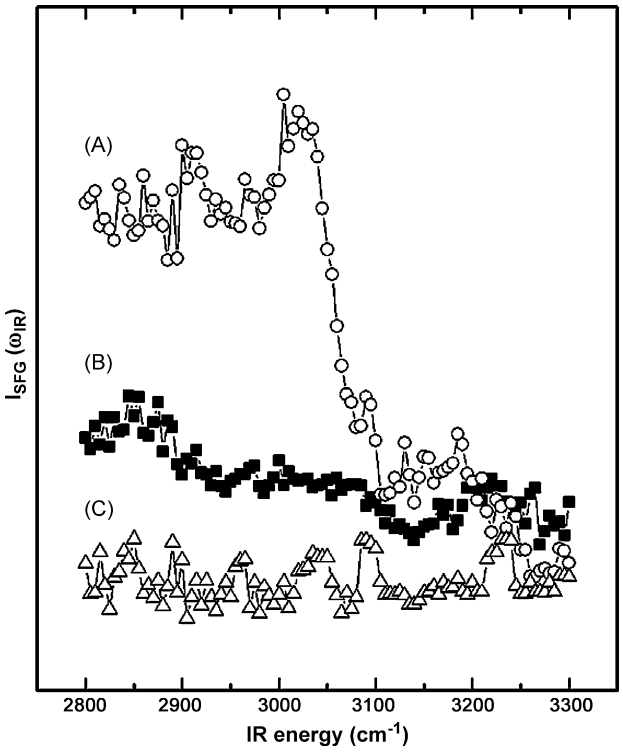

Fig. 1. Decomposition of 40 Torr CH_4 in the (A) absence of hydrogen and in the (B) presence of 10 Torr H_2 at 473 K. For reference, (C) is a SFG spectrum of clean Pt(5 5 7) under UHV conditions before the introduction of methane. At elevated temperatures, enhancement in the SFG spectra between 2800 and 3050 cm^{-1} is evident and most likely due to the presence of carbon and CH_x fragments on the surface. Comparison of spectrum (A) with both (B) and (C) suggest that an adsorbed fragment derived from methane is responsible for the enhanced SFG signal. The lack of clear resonance(s) is due to the disordered nature of this dehydrogenated overlayer. The simultaneous introduction of hydrogen with methane suppresses the amount of adsorbed methane fragments either by site blocking or rehydrogenation of the surface fragments.

3. Results and discussion

3.1. Non-oxidative decomposition of methane in the presence and absence of H_2 and CO

The adsorption and decomposition of methane on Pt(5 5 7) was studied with SFG and Auger electron spectroscopy. SFG has previously been used to identify dehydrogenated C_1 and C_2 fragments on Pt(1 1 1) from the decomposition of methane after heating the surface for 60 s to temperatures ≤600 K followed by cooling to 200 K [20]. Resonances for methyl and methylidyne, as well as a carbon coupling products, ethylidyne were observed at room temperature after heating to ~600 K and cooling. The SFG spectrum of the adsorption of CH_4 on Pt(5 5 7) at 673 K is shown in Fig. 1A. There are no observable resonances above 3100 cm^{-1} (compare with SFG spectrum of clean Pt(5 5 7), Fig. 1C), but from 2850 to 3050 cm^{-1}, there is a distinct enhancement of the SFG signal. The enhancement may be due to a non-resonance effect causing the visible light to interact more strongly with Pt(5 5 7) after CH_4 decomposition or a very weak resonance effect between multiple adsorbed species which are randomly oriented and in low concentrations. The exact cause of the spectral enhancement is unknown, but it certainly coincides with C–H resonances that could arise from CH_x and C_2H_x fragments. Analysis of the surface after cooling to room temperature and evacuation to ~10^{-8} Torr by AES indicates that the surface is covered with carbon, as identified by the large C(1s) peak at ~271 eV in Fig. 2A. The Auger spectrum of a clean Pt(5 5 7) crystal is shown in Fig. 2B. The atomic identity of the carbon is unknown, but most likely a mixture of atomic C and CH_x fragments. The relative coverage of carbon is calculated by a previously published method in which the intensity of the Pt (237 eV) peak is compared with the intensity of the 272 eV carbon peak [21]. Calculation of absolute carbon coverage requires prior knowledge of a saturation value of carbon atoms to Pt surface atoms. Therefore, the values listed in this text are relative to the unspecified areal density of C atoms in a saturation layer, but for comparative purposes, the values can be directly compared [22]. The inset in Fig. 2 demonstrates that the rate of methane decomposition is fast and decreases quickly (to zero) as the coverage saturates at ~0.6 monolayer (ML) at a surface temperature of 473 K. As the surface temperature increases, the saturation coverage approaches a full monolayer. It must be stated that the absolute coverage of carbon is difficult to

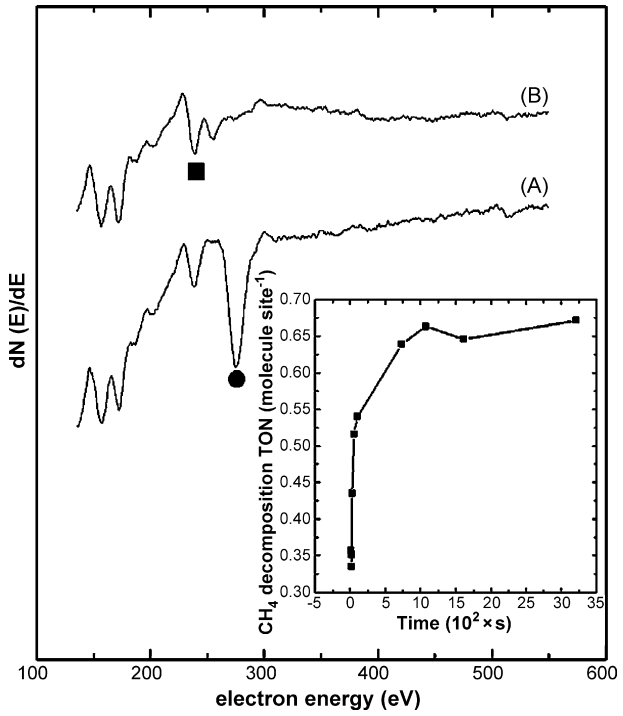

Fig. 2. Non-oxidative decomposition of methane on Pt(5 5 7). (A) Auger spectrum of a carbon covered surface after CH_4 decomposition (40 Torr) for 840 s at 473 K. The carbon coverage was determined by converting the ratio of the peak to peak intensities of the C(272 eV) (●) Auger peak to the Pt(237 eV) (■) Auger peak according to a previously published method [21]. (B) Auger spectrum of a clean Pt(5 5 7) single crystal before CH_4 decomposition. Inset is the kinetics of methane decomposition measured by AES at 473 K and 40 Torr CH_4.

determine because carbon can be present as either a carbidic or graphitic monolayer [22]. The carbidic phase saturates below a monolayer while the saturation coverage for the graphite is greater than a monolayer. For example, on Pt(1 1 1), the incommensurate graphite monolayer is 2.5–3 times the Pt(1 1 1) areal density assuming an areal density of 3.8×10^{15} cm^{-2} for a graphite monolayer [22,23]. Therefore, we are unable to comment on the type of carbon, although it has been demonstrated that annealing carbidic islands on Pt(1 1 1) converts them to graphite [24]. The role of step edges in the formation of carbon monolayers is discussed below.

Following the decomposition of methane by Auger analysis is limited by the temperature range (373–523 K) over which the rate (by carbon coverage) could be measured accurately. The empirical method used to calculate the carbon coverage is valid only up to a monolayer which was reached by 500–510 K. At high carbon coverage, an apparent activation energy, E_{app} of ~9 kcal mol^{-1} was measured, which is in good agreement with an activation energy of ~10 kcal mol^{-1} calculated for Pt(1 1 1) using molecular orbital methods [25]. A reported activation energy this low is consistent with previously reported SFG observations of methyl fragments on Pt(1 1 1) at room temperature [20]. A slightly higher activation energy of 11 kcal mol^{-1} was determined experimentally on Pt(1 1 0) [26]. Activation energies ranging from 8 to 11 kcal mol^{-1} on a series of flat, stepped and kinked Pd single crystals at 300–600 K and 1 Torr CH_4 were reported by Klier et al. [27]. More recent values for methane decomposition activation energies on Pt(1 1 1) are ~15 kcal mol^{-1} determined separately by an effusive molecular beam technique [22] and generalized gradient approximation density function theory (GGA-DFT) [28]. Frennet has also measured activation energies in this range for the decomposition of methane on a series of transition metal polycrystalline foils [29]. The reason for the low apparent energy may be related to the predominance of CH_4 decomposition at step sites [30] which are quickly covered during stoichiometric methane decomposition forcing the continued decomposition to take place on the less active (1 1 1) terraces. Molecular beam studies on Ir(1 1 1) [31], Ir(1 1 0) [32] and Pt(1 1 1) [33] demonstrated that surface defects increase the dissociation rate of methane. A significantly higher activation energy of 19.4 kcal mol^{-1} was calculated by bond order conversation methods [34]. It must be noted that these activation energies are measured at temperatures significantly lower than the temperature required for reforming reactions and may not represent energetics relevant to methane decomposition at reforming temperatures. Apparent activation energies (18.6 kcal mol^{-1}) of stoichiometric methane decomposition measured at reforming conditions on supported Pt crystallites were a factor of ~2 higher than all values reported on single crystal surfaces [7].

The addition of hydrogen or carbon monoxide led to decrease in methane decomposition. Fig. 1B is the SFG spectra for the decomposition of 40 Torr methane at 473 K with the addition of 10 Torr H_2. The SFG signal has decreased substantially for the IR region from 2850 to 3050 cm^{-1}, but is still not at the clean Pt(5 5 7) non-resonant background (Fig. 1C) signal suggesting that carbon fragments remain on the surface. The presence of residual carbon fragments on the crystal surface is confirmed by Auger electron spectroscopy (spectrum not shown). The addition of 2 Torr H_2 decreased the carbon coverage by ~75%, which decresed by ~82% with 10 Torr H_2. The actual role of hydrogen in preventing carbon accumulation as a site blocker or a source of hydrogen for rehydrogenation is unknown.

Addition of carbon monoxide led to decreased surface carbon accumulation due to site blocking by carbon monoxide. Unfortunately, the adsorption of CO on the step and terrace sites could be not be distinguished at room temperature due to rapid diffusion between these sites. Fig. 3A and B are SFG spectra of the CO stretch region in the absence of CH_4 and with 40 Torr CH_4 at 523 K, respectively. The 8 cm^{-1} red shift of the atop CO peak in the absence of methane is due to dipole coupling between neighboring CO, while in the presence of adsorbed carbon and CH_x fragments, dipole coupling between CO adsorbates is reduced. The inset demonstrates that there is no influence of methane on the temperature dependence of the atop CO stretch position until the temperature is ≥430 K, which corresponds to the desorption of CO from Pt(1 1 1) [35].

3.2. Kinetics of direct dry and steam reforming of methane on Pt(5 5 7): temperature and partial pressure dependence

The kinetics of steam and dry reforming of methane have been studied extensively over supported Pt crystallites [36–39]

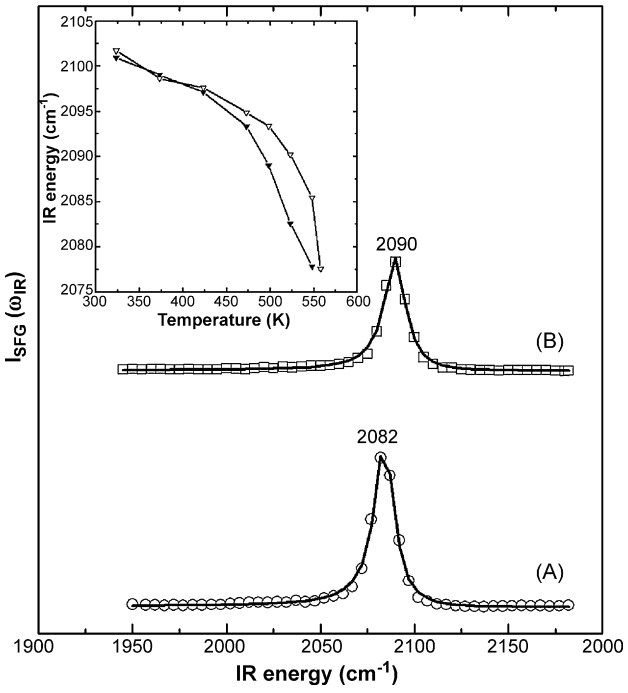

Fig. 3. SFG spectra of adsorbed carbon monoxide during methane decomposition. (A) SFG spectra of 10 Torr CO adsorbed to a clean Pt(5 5 7) at 523 K. The peak position of the atop CO band is in good agreement with previous results on a clean (5 5 7) crystal [15]. (B) SFG spectrum of atop CO adsorbed to Pt(5 5 7) in the presence of 40 Torr CH_4. The peak position of carbon monoxide is 2090 cm^{-1} indicative of less dipole coupling compared to the situation in spectrum (A) suggesting that CH_x fragments derived from methane decomposition influence the surface chemistry of adsorbed carbon monoxide. The inset demonstrates the influence of surface temperature in the absence of CH_4 (closed symbols) and in the presence of 40 Torr CH_4 (open symbols) on the peak position of adsorbed CO.

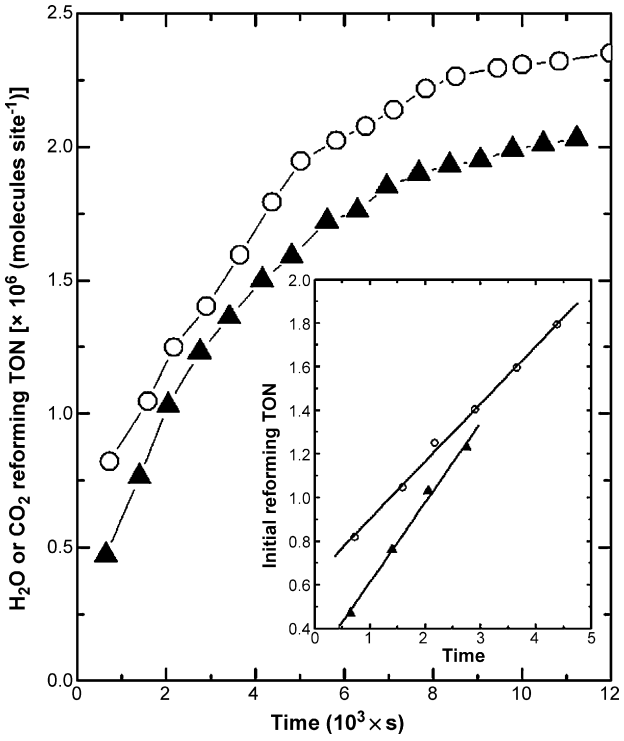

Fig. 4. Accumulation plots for (▲) direct CO_2 reforming of CH_4 and (○) direct H_2O reforming of CH_4 at 973 K. Reaction conditions were 200 Torr CH_4, 40 Torr CO_2 or 20 Torr H_2O. The inset demonstrates the calculation of the initial turnover rate. The constant slope with time is consistent with differential reactor conditions with no catalyst deactivation or poisoning.

but no studies with Pt single crystals were found. Most studies employ stoichiometric or near stoichiometric mixtures of CH_4 and H_2O or CO_2. Industrial steam reformers run at excess steam to limit the amount of carbon deposition [4]. The initial turnover frequency for both direct reforming reactions was measured under fuel rich conditions (200 Torr CH_4, 40 Torr CO_2 or ~20 Torr H_2O). Fig. 4 is an accumulation plot of CO for both reactions at 973 K. The rate of steam reforming was a factor of ~1.5 times higher than CO_2 reforming at comparable partial pressures. Initial rates for both reforming reactions are listed in Table 1. The rate of steam reforming was extrapolated from 20 Torr (highest H_2O partial pressure obtainable with reactor set up) to 40 Torr assuming a linear dependence of the reforming rate on H_2O pressure. The inset of Fig. 4 demonstrates the initial behavior of the accumulation curve for both reactions. The accumulation of CO during steam reforming was linear for longer times suggesting the rate of carbon deposition on Pt(5 5 7) was slower than during dry reforming. Shortened catalyst lifetimes due to carbon deposition are well-known for both reactions, but are generally shortened to a greater extent with dry reforming catalysts [40].

The apparent activation energies, E_{app} were measured for both co-reactants during methane reforming. Arrhenius plots for both reactions are shown in Fig. 5 and apparent activation

Table 1
Turnover rates and kinetic parameters for the combined oxidation-reforming of methane on Pt(5 5 7)

Reaction	CH_4 turnover rate[a]	CO turnover rate (s^{-1})[a]	E_{app} (kcal mol^{-1})[b]	Reaction orders for CO production[c]			
				CH_4	O_2	CO_2	H_2O
CO_2 reforming	370	370	32	0.01	–	0.96	–
H_2O reforming	520	520	29	0.04	–	–	0.99
Combined oxidation-reforming	1360	550	24	0.32 (−0.03)[d]	0.08 (1.3)[d]	–	–

[a] Standard reaction conditions of 200 Torr CH_4, 30 Torr O_2 (40 Torr CO_2 or 20 Torr H_2O), and 973 K. Rates [in table] for steam reforming were corrected to 40 Torr H_2O from 20 Torr using the measured first order dependence on H_2O partial pressure.
[b] Same pressure conditions as listed in (a) and 950–1050 K.
[c] Reaction conditions are stated in Fig. 8 caption for CH_4–O_2 reaction; 100–200 Torr CH_4, 40–160 Torr CO_2 and 973 K, 200 Torr CH_4, 40–160 Torr CO_2 and 973 K for the CH_4–CO_2 reaction; 100–200 Torr CH_4, 10 Torr H_2O and 973 K, 200 Torr CH_4, 8–20 Torr H_2O and 973 K for CH_4–H_2O reaction.
[d] Reaction orders in CH_4 and O_2 for CO_2 formation. Conditions are stated in Fig. 8 caption.

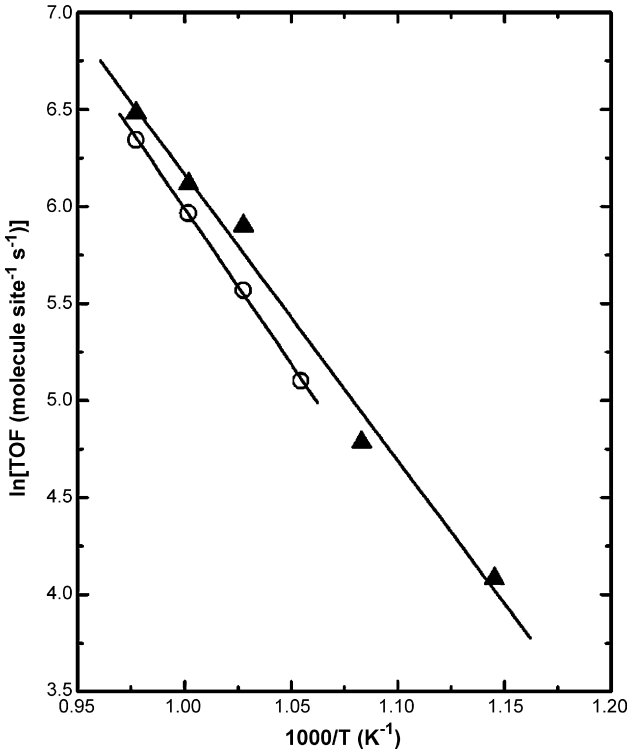

Fig. 5. Arrhenius plot for (▲) direct CO_2 reforming of CH_4, and (○) direct H_2O reforming of CH_4. The apparent activation energy for the CO_2 and H_2O reforming of CH_4 were 29 and 32 kcal mol^{-1}, respectively. The reaction conditions were 200 Torr CH_4, 40 Torr CO_2 or 20 Torr H_2O and 923–1073 K.

energies are listed in Table 1. Apparent activation energies of steam and dry reforming were 29 and 32 kcal mol^{-1}, respectively. The similarities in activation energy suggest that a common rate determining step exists between the two reactions as previously proposed [9]. The difference in E_{app} between reactions may be related to differences in the thermodynamics of co-reactant adsorption on carbon covered surfaces. Compared with E_{app} measured on supported catalysts, those reported here are significantly larger. Activation energies on supported catalysts ranging from ∼14 to 25 kcal mol^{-1} [41,42] are typically reported, although values as high as 33–35 kcal mol^{-1} have been reported for Pt/MgO catalysts [9,43]. These values are apparent activation energies—representing both the activation energy of the rate determining step and adsorption energies of any kinetically relevant co-reactants.

Partial pressure dependencies during steam and methane reforming have primarily been studied at similar partial pressure of methane and CO_2 or H_2O. In this study, fuel rich (∼10 fold excess CH_4) conditions led to zero order methane kinetics for both reactions and first order kinetics in both CO_2 and H_2O. Partial pressure dependencies for both reforming co-reactants are compiled in Table 1. The zero order dependence on methane suggests that surface is covered with C and CH_x fragments formed through the sequential dehydrogenation of methane [44]. The measured kinetic dependencies suggest that the large coverage of methane derived species influences the adsorption of both CO_2 and H_2O to the same extent; both co-reactants display first order behavior. In the experimental conditions utilized in this study, the reaction can be written as a power rate law, $r = k_{app}P_{CO_2(\text{or } H_2O)}$. The observed power rate law differs from one recently proposed [7,8]; reforming rates are proportional to CH_4 partial pressure and independent of the co-reactant (H_2O or CO_2) at approximately 1:1 CH_4 to co-reactant feed. In this study, the authors concluded that any one of the sequential methane dehydrogenation steps was rate determining step, while the adsorption of either CO_2 or H_2O was quasi-equilibrated and kinetically irrelevant. After adsorption and dissociation of CO_2 to adsorbed CO* (where * = surface Pt atom) and O*, CO desorbs and O* reacts with C* from methane. The four hydrogen atoms of methane recombine to form two H_2 molecules to complete the stoichiometry of the overall reaction. A similar sequence of elementary steps occurs during steam reforming: water dissociates to H* and OH*, which further reacts with C* and H* to form CO and H_2. The authors conclude that surface must be essentially bare of methane derived reactive intermediates, otherwise higher CO_2 (or H_2O) pressures would increase the reaction rate. In this study, the opposite situation is postulated; the surface is covered with reactive carbon deposits which are removed at a higher rate as the CO_2 (or H_2O) pressure is increased. The high partial pressure of methane leads to a favorable CH_4 adsorption equilibrium, resulting in a high coverage of CH_x fragments. In this case, a complex rate expression is reduced to a power rate law because the site balance is reduced to CH_x fragments, whose coverage is proportional to the CH_4 pressure. This reduces the overall dependence of CH_4 to zero order. Bradford and Vannice have recently reviewed proposed mechanisms for both dry and steam reforming of methane over supported metal catalysts [5]. Significantly more complex partial pressure dependencies during dry reforming have been reported by Bradford and Vannice [41] on supported Pt catalysts and by Solymosi and co-workers [45] on supported Ir catalysts. Differences in observed partial pressure dependencies led to the proposal that adsorbed CH_x combine with O* species to form CH_xO fragments which eventually decompose to CO* and xH*. The proposed sequence of elementary reaction steps and site balance led to a complex Langmuir–Hinshelwood type rate expression that sufficiently fit the experimental data. Rostrup-Nielsen and Hansen have previously proposed that it is unlikely the mechanism of dry reforming differs significantly from that of steam reforming [9]. The same authors have shown that the mechanism between H_2O and CO_2 differs on Ru/MgO catalysts, presumably due to the higher barrier for CO_2 activation resulting in this activation step becoming rate determining [9]. We prefer the mechanism proposed by Wei and Iglesia [7] due to its relative simplicity, but the differences between our observed kinetics and those of previously reported studies suggest that the true kinetic expression is more complex than either of the limiting cases—high carbon coverage and low carbon coverage.

3.3. Kinetics of combined total oxidation and reforming of methane on Pt(5 5 7)

The kinetics of low temperature (623–673 K) total combustion and the reforming of both the CO_2 and H_2O formed during the combustion were examined. Fig. 6 is an

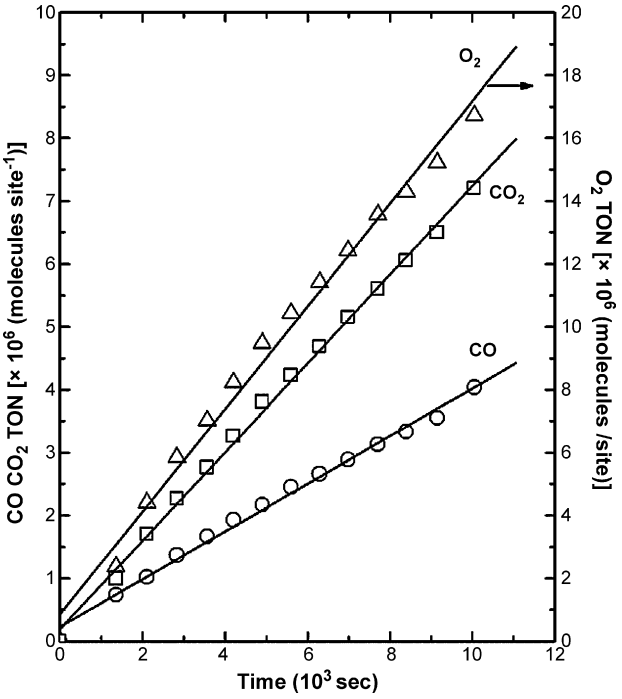

Fig. 6. Accumulation of CO/CO_2 and disappearance of O_2 with time during combined oxidation-reforming of methane. Reaction conditions are 300 Torr CH_4, 30 Torr O_2 and 923 K. The conversion of methane never exceeded 5%, while oxygen conversions as high as 30% were achieved at reaction times greater than 10^4 s and temperatures greater than 998 K.

accumulation plot for CO_2 and CO at 300 Torr CH_4, 30 Torr O_2 and 973 K. At these conditions, both CO_2 and CO are observed in the GC after the first injection (∼1300 s of reaction). The turnover rates to CO and CO_2 were 550 and 810 s^{-1}, respectively at 973 K under fuel rich conditions (10:1 CH_4:O_2 ratio). The rate of O_2 disappearance with time is also included in Fig. 6. The rate of O_2 disappearance is 1.4×10^3 s^{-1}, slightly higher than the combined rate of CO and CO_2 generation assuming all CO comes from the reforming of CH_4 by combustion products and no direct partial oxidation occurs. These rates are believed to be kinetically controlled as the single crystal surface is non-porous and the high recirculation rates (∼1000 cm^3 min^{-1}) duplicate a well mixed batch reactor. The total conversion of methane under these conditions is ∼3.5%. An oxygen mass balance (with no attempt to quantify the amount surface oxygen) demonstrates that ∼4% of the oxygen reacted is not accounted for. The current experimental set up does not allow for the detection of H_2O and this source of missing oxygen may be that which reacts with H_2 to form water. Supported Pt catalysts generally suffer poor H_2 selectivity due to strong affinity for hydroxyl combination with H*. However, if the missing oxygen is located on the surface; this oxygen may enable the Pt surface to turnover faster than either reforming reactions and oxidize surface carbon negating deactivation from carbon deposition. Comparison of Figs. 4 and 6 demonstrates the CH_4/O_2 reaction shows no signs of deactivation even after 3 h of reaction. Increased stability of the catalyst due to the addition of oxygen to CH_4/CO_2 feedstock has been observed previously on supported catalysts [46,47].

The temperature dependence was examined over a large range (623–1050 K) and the results are shown in Fig. 7. At low temperatures (data to right of arrow in figure), only CO_2 was observed due to the total combustion of CH_4. Low temperature measurements (623–673 K) of CH_4 total combustion were carried out in the high pressure, low volume reaction cell. Conversions as high as 20% based on methane were achieved but all reported rates are initial. The apparent activation energy for CH_4 combustion under fuel rich conditions was 24.2 kcal mol^{-1}. The apparent activation energy previously reported for a Pt foil under fuel lean conditions (O_2:CH_4 = 10) was 32 kcal mol^{-1} [48]. The difference in reaction conditions or differences in the active site may be the cause of the lower apparent activation energy on Pt(5 5 7). In separate studies, fuel lean apparent activation energies of 21 and 28 kcal mol^{-1} have been reported on Pt wire and Pt black, respectively [49,50]. No carbon monoxide was detected at these lower temperatures.

As the temperature is increased above 698 K, the rate of CO_2 production is less sensitive to changes in temperature and at higher temperatures, the CO_2 production rate decreases with increasing temperature. Over the intermediate temperature range (698–923 K), the rate of CO_2 production decreased but no CO was detected in the gas phase. The apparent activation energy over this temperature range was ∼2 kcal mol^{-1}. It is not believed that this an indication of a mass transfer controlled

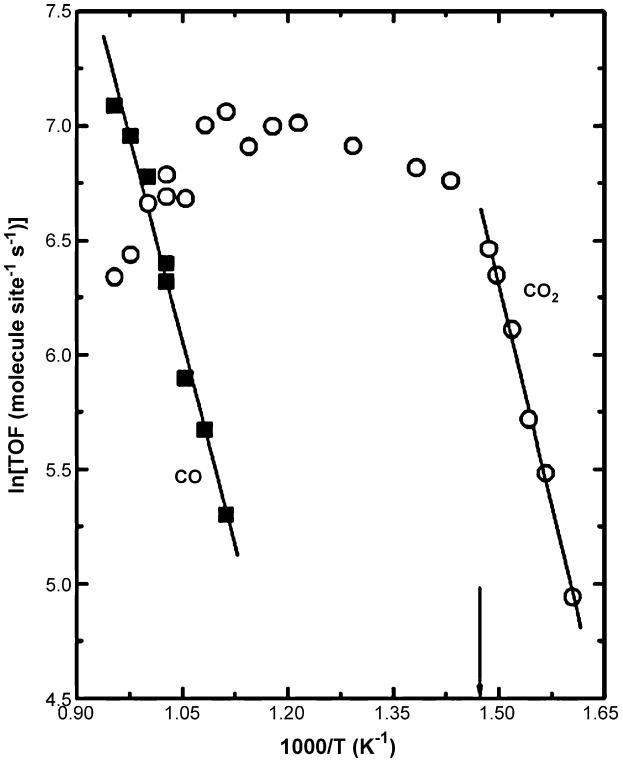

Fig. 7. Arrhenius plot for combined oxidation-reforming of methane. The apparent activation energy for CO formation is 23.6 kcal mol^{-1}. Reaction conditions were 300 Torr CH_4, 30 Torr O_2 and 823–1050 K. All methane conversions were ≤5% and oxygen conversions never exceeded 30% for any set of experimental conditions. Experiments to the right of the arrow were performed in a low volume (350 mL) reactor. CO_2 was the only detectable product to the right of the arrow.

reaction but instead an issue of CO detection or the involvement of CO in either water gas shift, methanation or oxidation chemistry. These intermediary temperature reactions were run in the 35 L bell jar. As the measured rate of CO_2 production decreases considerably, the rate of CO_2/H_2O reforming to produce CO increases. The apparent activation energy for CO production from CH_4/O_2 through a reforming pathway is 24 kcal mol^{-1} (Fig. 7). It is interesting to note that on Pt(5 5 7), the apparent activation energy for CO_2 formation in the total combustion regime and CO formation in the reforming regime are identical, suggesting that the same rate determining step applies and the heat of adsorption associated with the co-reactant (i.e. O_2, H_2O and CO_2) are similar under these experimental conditions. This would suggest that the reaction between either surface carbon or CH_x ($1 \leq x \leq 3$) and adsorbed oxygen, O* is the rate determining step, where O* originates from gaseous oxygen. The identity of the co-reactant does not influence the barrier and the only role of the co-reactant is to supply the surface with oxygen.

In the combined combustion-reforming regime under fuel-rich conditions, the dependence on O_2 is 1.27, while the methane order is slightly negative (−0.03) for CO_2 formation, which suggests that the Pt(5 5 7) surface is covered with carbon and CH_x fragments (Fig. 8). The partial pressure dependence on oxygen for the formation of CO is ∼0.08, while the dependence on methane is 0.32. It is difficult to rationalize the fractional dependence on methane partial pressure in this case, but in the case of oxygen, the zero order dependence suggests that oxygen is not directly involved in the formation of CO. This is further supported by the influence of O_2 pressure on CO selectivity. The influence of temperature at constant O_2 pressure (30 Torr O_2) and O_2 partial pressure at 973 K on CO selectivity is shown in Fig. 9. Selectivities were determined from the initial turnover frequencies. As expected, CO selectivity increased with temperature due to an increased rate of CO_2 and H_2O reforming, while the increase in oxygen led to a decrease in CO selectivity most likely due to the inability of adsorbed CO to desorb without reoxidation to CO_2 or the inability for combustion products CO_2 and H_2O to readsorb and reform. The H_2 selectivity cannot be assessed due to the inability to monitor both H_2 and H_2O concentrations. Similar to the influence of increased O_2 partial pressure on lowering CO selectivity, it is highly likely that competing H_2 oxidation would decrease H_2 selectivity. It may be that an appropriate partial pressure and residence time (when operating in a flow reactor) are required to optimize both catalyst lifetime and syngas selectivity. Thermodynamic calculations at 1 bar and 1073 K demonstrate that methane conversions up to 90% and syngas selectivities up to 97% are attainable under partial oxidation conditions [51]. Schmidt has reported syngas selectivity as high as 90 and 75% in microsecond contact time reactors containing Rh and Pt catalyst, respectively [52].

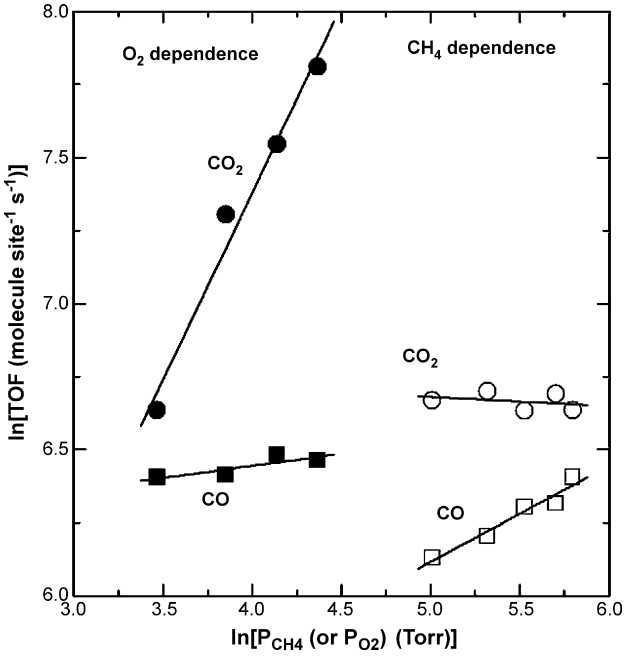

Fig. 8. Reaction orders in methane (open symbols) and oxygen (solid symbols) for the formation of CO and CO_2 during combined oxidation-reforming of CH_4. Reaction conditions were 200–330 Torr CH_4, 30 Torr O_2 and 973 K, and 300 Torr CH_4, 30–80 Torr O_2 and 973 K.

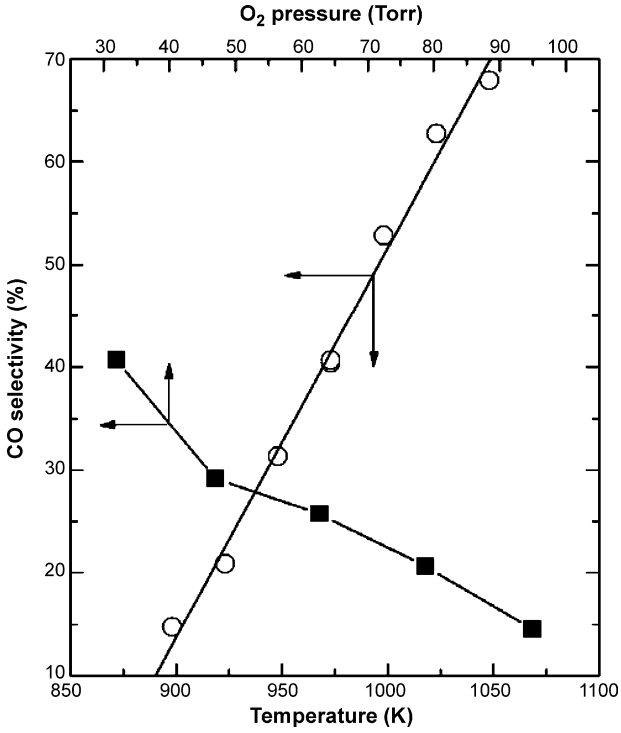

Fig. 9. Influence of temperature and oxygen pressure on CO selectivity during combined oxidation-reforming. Reaction conditions were 300 Torr CH_4, 30 Torr O_2 and 900–1050 K. The dependence on O_2 partial pressure was examined at 300 Torr CH_4, 30–100 O_2, and 973 K.

3.4. Characterization of Pt(5 5 7) single crystal after dry reforming and combined combustion-reforming

Both direct reforming reactions suffer from severe catalyst deactivation due to carbon deposition. Rostrup-Nielsen and Hansen demonstrated that the amount of carbon deposition on metal supported catalysts increased in the order

Ni > Rh > Ru > Ir > Pt at 773 K, but at a more relevant reforming temperature (923 K), the greatest quantity of carbon was deposited on Pt compared with the above mentioned metals [9]. Addition of a second metal which is inert to methane activation has proven a useful strategy to limit or even eliminate carbon deposition. Small amounts of Au addition to a supported Ni catalyst eliminated catalyst deactivation due to carbon deposition during the steam reforming of *n*-butane [53]. Catalyst deactivation by carbon deposited can be controlled by tuning support oxygen reactivity or the oxygen storage capacity of the support. Cerium or lanthanum promotion to Pt/ZrO_2 increased catalyst stability due to the higher density of oxygen vacancies on the promoted support, which favors a cleaning mechanism of the metal particle [54].

In this study, ex-situ analysis of the Pt(5 5 7) single crystal surface after both direct CO_2 reforming and combined combustion-reforming demonstrated significantly more carbon was deposited during CH_4/CO_2 than CH_4/O_2 reactions. Quantification of carbon coverage was determined from Auger analysis using the method described in Section 3.1. Auger spectra after CO_2 reforming and combined oxidation-reforming are shown in Fig. 10. After reaction for similar total time (~3 h), the amount of carbon is significantly higher on the surface after CH_4–CO_2 reforming. Carbon coverage after CO_2 reforming was ~1.2 ML, while the coverage after combined combustion-reforming was ~0.6 ML. In the latter reaction, the atomic C:O ratio in the beginning reaction mixture is 1/2, while for dry reforming, the same ratio is unity.

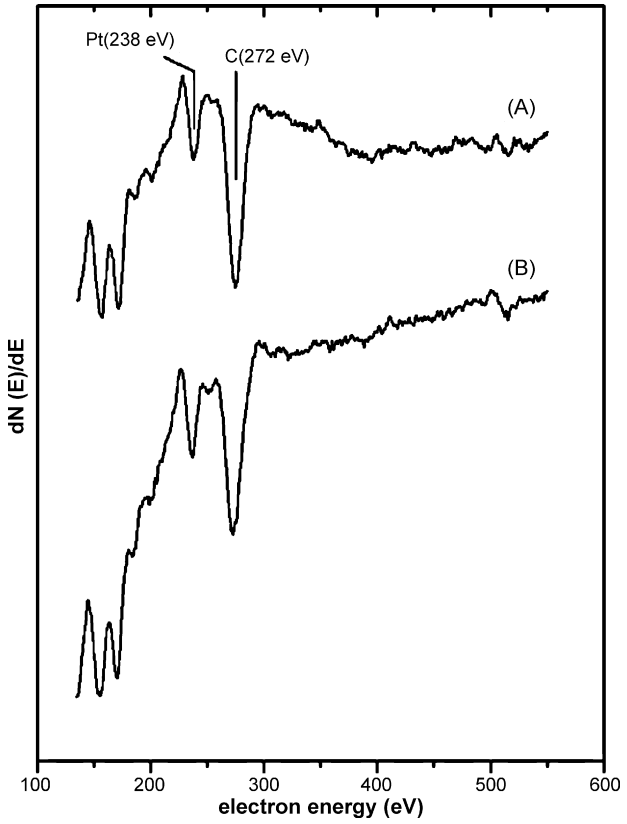

Fig. 10. AES spectra of carbon region after (A) direct dry reforming and (B) combined oxidation-reforming of CH_4. There is significantly less carbon deposition during the combined oxidation-reforming of methane than in the case of either direct reforming reactions or the non-oxidative decomposition of methane (see Fig. 2A). The number of carbon monolayers for dry reforming at the end of a 11 ks batch reaction was greater than a monolayer (estimated at 1.2 ML) while the carbon coverage for a similar reaction time for the combined oxidation-reforming of methane was 0.6 ML. All Auger spectra were collected after evacuation of reactor to $\sim 1 \times 10^{-8}$ Torr. There may be a small amount of adsorbed oxygen ($O_{(1s)}$ = 530 eV) on the Pt(5 5 7) surface after combined oxidation-reforming.

The significantly lower carbon coverage on this surface is most likely due to the higher concentration of O* species at the step edges due to increased adsorption energy at steps [55,56]. Step sites are believed to be the site for carbon nucleation [57], and high resolution electron microscopy studies have shown that graphene layers grow from surface steps which then migrate with the growing sheet [58]. The stronger adsorption of oxygen to the step sites may limit carbon deposition by eliminating the nucleation site for graphene formation. Adsorbed oxygen will also scavenge the surface and oxidize any surface carbon $C_{(s)}$ according to the following reaction,

$$xO_2 + C_{(s)} \rightleftarrows 2(x-1)CO + (2x-1)CO_2 \quad (1)$$

The CO_2 generated in this cleaning step can reenter the catalytic cycle leading to the introduction of another O atom to the surface pool by the equilibrated decomposition of CO_2 to CO* and O*. The addition of steam during dry reforming increases catalyst lifetime by carbon gasification pathways [5] (see Eq. (2)) and serves as an additional reaction pathway for carbon removal during combined oxidation-reforming.

$$H_2O + C_{(s)} \rightleftarrows CO + H_2 \quad (2)$$

It has been suggested that carbon deposition during reforming is due to both methane decomposition and CO disproportionation ($2CO \rightarrow C_{(s)} + CO_2$). Auger analysis of the Pt(5 5 7) after 30 min (2 injections) on stream (CH_4/CO_2, 973 K) confirmed a carbon coverage of 0.75 ML, demonstrating that carbon deposition occurs in the initial stages of reaction under conditions where the CO partial pressure is extremely low. CO disproportionation is exothermic and becomes unfavorable above 973 K [59]. Addition of excess CO to both steam and CO_2 reforming supported Pt catalysts had no influence on the observed catalyst activity or stability, confirming CO readsorption under reforming conditions is unfavorable [7]. This was confirmed on the Pt(5 5 7) single crystal by the addition of 5 Torr CO which had no influence on the amount of carbon deposition during dry and steam reforming.

The additional exothermic reaction pathway (i.e oxidation) for surface carbon removal in the case of combined combustion-reforming is most likely responsible for the lower carbon coverage. From the Auger spectrum (Fig. 10B), it appears that a small amount of oxygen is present on the surface, which could represent the oxygen unaccounted for from the gas phase oxygen mass balance (see Section 3.3). It is proposed that CO_2 adsorbs and dissociates into CO* and O* during dry reforming and in a similar manner H_2O dissociates to H* and *OH during steam reforming, while during combined

combustion-reforming, the surface pool of oxygen surface species, O* will not only control the carbon coverage by oxidation to CO or CO_2 (Eq. (2)), the CO_2 formed during the process can participate in the dry reforming catalytic cycle.

Connor and Ross have shown that the loss of catalytic activity during CO_2 reforming on Pt/ZrO_2 catalysts decreased as more oxygen was added to feed [46]. The authors found that upon addition of 9 vol.% O_2 to CH_4/CO_2 (ratio: 4/1) inlet stream, the amount of carbon deposition was still zero after 6 h on stream at 1073 K, while the catalyst subjected to a feed stream with no oxygen continued to gain weight with time on stream due to carbon deposition. Similar behavior has been documented for Ni/CaO catalysts [60]. It has been proposed that the coverage of reactive carbon deposits under stoichiometric reforming conditions (without O_2) must be very low as deduced from reaction kinetics because increases in both steam or CO_2 partial pressure had little influence on the reaction rate [7,8]. In this study, we are operating in a different kinetic regime in which the rate is directly proportional to steam, CO_2 or O_2 partial pressure. This demonstrates that the surface of the Pt(5 5 7) single crystal is covered with reactive carbonaceous residues. The observations from this study are in contrast to the work by Wei and Iglesia [7,8] possibly due to the difference in reaction stoichiometry or the role of oxide support during the reaction. The oxide support may be play a very important in carbon removal by providing surface or lattice oxygen to oxidize solid carbon to CO [41] or possibly as a sink for these carbonaceous residues by a reverse spillover mechanism [61]. This carbon removal pathway is not accessible on the single crystal and may be a potentially important route for carbon removal on industrial catalysts.

3.5. Methane to syngas in the presence of oxygen: direct or indirect pathway or a combination of both

It has been proposed that methane partial oxidation to CO and H_2 proceeds in two steps. First, methane is totally oxidized by oxygen to yield CO_2 and H_2O, which subsequently reforms the unreacted methane to synthesis gas (indirect mechanism). In the direct mechanism, O* recombines with adsorbed carbon to form CO and adsorbed H recombine to form H_2. This study suggests that syngas formation from CH_4/O_2 on Pt is due to an indirect pathway. No CO formation was observed without the presence of carbon dioxide in the gas phase. The inability to detect both H_2 and H_2O doesn't enable the assessment of reactions involving hydrogen, mainly H_2 oxidation and the reverse water gas shift reaction, which has been shown to be equilibrated at reforming conditions [5,7]. Based on short contact time reactor measurements, the selectivity to H_2 on Pt is much lower than CO selectivity due to the oxidation of hydrogen to water [52].

Isotope studies (CH_4/CO_2 and CD_4/CO_2) suggested that two CO formation pathways exist during CO_2 reforming. The formation of CO was influenced to a lesser extent by an isotope effect (compared with normal deuterium isotope effect seen with the methane conversion rate), suggesting that a portion of gas phase CO is formed directly from the dissociation of CO_2 to gaseous CO and adsorbed oxygen, which further participates in the oxidation of $C_{(s)}$ or CH_x fragments [62]. In a separate study of CH_4/CD_4 isotope effect on the partial oxidation of methane to syngas, the results support a parallel mechanism in which CO_2 and CO form simultaneously; the reaction of surface carbon leads to CO_2 formation and the reaction of CH_xO surface species with adsorbed oxygen led to CO formation [63]. This direct partial oxidation pathway differs from a direct mechanism proposed by Schmidt and co-workers for partial oxidation of CH_4 over monolithic Rh and Pt in short contact time (10^{-3} s) reactors. Hickman and Schmidt propose that oxygen scavenges the surface of carbon to form CO and the hydrogen liberated during the decomposition of methane desorbs into the gas phase [52]. No carbon dioxide formation was observed during a supersonic molecular beam study of methane partial oxidation on Rh(1 1 1) suggesting that a direct mechanism may be applicable under single collision conditions [64].

The concentration of adsorbed oxygen (O*) plays a crucial role in the observation of CO and H_2 as primary products. Transient pulse experiments by Weng et al. [65] suggest that only a narrow concentration of O* leads to CO formation (by a direct pathway). At optimal O*, CH_4 dissociation is fast, while at oxygen coverages greater than optimal, CH_4 adsorption is hindered [66], and CO and H_2 are oxidized to the combustion products before desorption. Even under the reaction conditions employed here, the coverage of oxygen is presumably low based on the observed kinetics and ex-situ Auger analysis, but an indirect mechanism is mostly like appropriate.

The pathway (direct or indirect) for syngas formation from CH_4 and O_2 at high temperatures is still unknown. Single crystals represent the optimal substrate to determine the influence of the metal identity and structure on the pathway without interference from a support [67]. It is difficult to assess the pathway only from the gas phase composition as numerous thermodynamically and kinetically favorable competing and side reactions are occurring. Spectroscopic techniques are of little to utility during these reactions because of the high temperatures and low concentrations of active species. Most likely, the only way to interrogate the pathway and mechanism of this complex chemistry is through isotope methods. A combined study of CH_4/O_2 high temperature conversion using isotopes and single crystal surfaces is necessary to determine the influence of surface structure on the mechanism of syngas formation. Work is undergoing in our laboratory to determine the pathway for syngas formation on both open (5 5 7) and close packed (1 1 1) Pt single crystal surfaces.

4. Conclusions

The non-oxidative decomposition and reforming of methane was studied on a stepped Pt single crystal. The kinetics of methane decomposition were followed by Auger electron spectroscopy. The reaction kinetics for both H_2O and CO_2 reforming of methane were measured as a function of temperature and reactant partial pressures. Rates for both dry and steam reforming were identical under similar reaction

conditions. The structure of the co-reactant had little mechanistic influence on the conversion of methane to carbon monoxide and hydrogen. Ex-situ examination of the surface showed carbon buildup after either reforming reaction was similar to the non-oxidative decomposition experiments, suggesting that carbon deposition is solely due to methane decomposition and H_2O or CO_2 mainly serve to scavenge the surface for adsorbed dehydrogenated or atomic carbon. The combined total oxidation of methane with dry and steam reforming of the methane led to CO and H_2 production rates which were a factor of 1.5–2 higher than direct reforming rates at similar conditions. The onset of methane reforming occurred at much lower temperatures in the presence of oxygen. The higher heat of adsorption of oxygen on step sites may block the deposition of residual carbon from the step edges and inhibit the formation of a graphitic monolayer resulting in a rate enhancement and high catalyst stability. Ex-situ Auger spectroscopy analysis demonstrates less carbon is deposited on the Pt single crystal surface during combined total oxidation-reforming.

Acknowledgements

This work was supported by the Director, Office of Science, Office of Advanced Scientific Computing Research, Office of Basic Energy Sciences, Materials Sciences and Engineering Division, of the U.S. Department of Energy under Contract No. DE-AC02-05CH11231. R.M.R. acknowledges the Ford Motor Company for financial support through a graduate fellowship administered by the Berkeley Catalysis Center. A.L.M. acknowledges the Donors of the American Chemical Society Petroleum Research Fund for support in the form of an Alternative Energy Postdoctoral Fellowship.

References

[1] J.H. Lunsford, Catal. Today 63 (2000) 165.
[2] G.A. Olah, A. Goeppert, G.K. Surya Prakash, Beyond Oil and Gas: The Methanol Economy, Wiley-VCH, Weinheim, 2006, p. 6.
[3] T. Koerts, A.R. van Santen, J. Chem. Soc. Chem. Commun. 18 (1991) 1281.
[4] M. Belgued, P. Pareja, A. Amariglio, Nature 352 (1991) 789.
[5] M.C.J. Bradford, M.A. Vannice, Catal. Rev. Sci. Eng. 41 (1999) 1.
[6] A.M. Gadalla, B. Bower, Chem. Eng. Sci. 43 (1988) 3049.
[7] J. Wei, E. Iglesia, J. Phys. Chem. B 108 (2004) 4094.
[8] J. Wei, E. Iglesia, J. Catal. 224 (2004) 370.
[9] J.R. Rostrup-Nielsen, J.-H. Bak Hansen, J. Catal. 144 (1993) 38.
[10] C.H. Bartholomew, Catal. Rev. Sci. Eng. 24 (1982) 67.
[11] P. Aghalayam, Y.K. Park, D.G. Vlachos, in: J.J. Spivey (Ed.), Catalysis, vol. 15, The Royal Society of Chemistry, 2000, p. 98.
[12] K. Heitnes, S. Lindberg, O.A. Rokstad, A. Holmen, Catal. Today 24 (1995) 211.
[13] M. Prettre, C. Eichner, M. Perrin, Trans. Faraday Soc. 43 (1946) 335.
[14] H.R. Siddiqui, P.J. Chen, X. Guo, J.T. Yates Jr., J. Chem. Phys. 92 (1990) 7690.
[15] K.R. McCrea, J.S. Parker, P. Chen, G.A. Somorjai, Surf. Sci. 494 (2001) 238.
[16] K.R. McCrea, J.S. Parker, G.A. Somorjai, J. Phys. Chem. B 106 (2002) 10854.
[17] K.R. McCrea, Ph.D. Thesis, University of California, Berkeley, 2002.
[18] S.J. Kweskin, K. Komvopoulos, G.A. Somorjai, Langmuir 21 (2005) 3647.
[19] M.B. Raschke, Y.R. Shen, Curr. Opin. Solid State Mater. Sci. 8 (2004) 343.
[20] A.L. Marsh, K.A. Becraft, G.A. Somorjai, J. Phys. Chem. B 109 (2005) 13619.
[21] J.P. Biberian, G.A. Somorjai, Appl. Surf. Sci. 2 (1979) 352.
[22] K.M. DeWitt, L. Valadez, H.L. Abbott, K.W. Kolasinski, I. Harrison, J. Phys. Chem. B 110 (2006) 6705.
[23] H. Ueta, M. Saida, C. Nakai, Y. Yamada, M. Sasaki, S. Yamamoto, Surf. Sci. 560 (2004) 183.
[24] T.A. Land, T. Michely, R.J. Behm, J.C. Hemminger, G. Cosma, J. Chem. Phys. 97 (1992) 6774.
[25] A.B. Anderson, J.J. Maloney, J. Phys. Chem. 92 (1988) 809.
[26] P.D. Szuromi, J.R. Engstrom, W.H. Weinberg, J. Phys. Chem. 89 (1985) 247.
[27] K. Klier, J.S. Hess, R.G. Herman, J. Chem. Phys. 107 (1997) 4033.
[28] A. Michaelides, P. Hu, J. Am. Chem. Soc. 122 (2000) 9866.
[29] A. Frennet, Catal. Rev. Sci. Eng. 10 (1974) 37.
[30] Y. Wang, R.G. Herman, K. Klier, Surf. Sci. 279 (1992) 33.
[31] D.F. Johnson, W.H. Weinberg, J. Chem. Phys. 101 (1994) 6289.
[32] D. Kelly, W.H. Weinberg, J. Vac. Sci. Technol. A 15 (1997) 1663.
[33] J.F. Weaver, M.A. Kryzowski, R.J. Madix, Surf. Sci. 391 (1997) 150.
[34] C.-T. Au, C.-F. Ng, M.-S. Liao, J. Catal. 185 (1999) 12.
[35] F.M. Hoffman, Surf. Sci. Rep. 3 (1983) 107.
[36] S.M. Stagg, E. Romeo, C. Padro, D.E. Resasco, J. Catal. 178 (1998) 137.
[37] K. Nagaoka, K. Seshan, J.A. Lercher, K. Aika, Catal. Lett. 70 (2000) 109.
[38] Y. Chen, B. Liaw, C. Kao, J. Kou, Appl. Catal. A Gen. 217 (2001) 23.
[39] M.M.V.M. Souza, D.A.G. Aranda, M. Schmal, J. Catal. 204 (2001) 498.
[40] T. Inui, in: J.J. Spivey (Ed.), Catalysis, vol. 16, The Royal Society of Chemistry, London, 2000, p. 133.
[41] M.C.J. Bradford, M.A. Vannice, J. Catal. 173 (1998) 157.
[42] F. Solymosi, Gy. Kustán, A. Erdöhelyi, Catal. Lett. 11 (1991) 149.
[43] D. Qin, J. Lapszewicz, Catal. Today 212 (1994) 551.
[44] C. Au, C. Ng, M. Liao, J. Catal. 185 (1999) 12.
[45] A. Erdöhelyi, K. Fodor, F. Solymosi, Stud. Surf. Sci. Catal. 107 (1997) 525.
[46] A.M. O'Connor, J.R.H. Ross, Catal. Today 46 (1998) 203.
[47] M.M.V.M. Souza, M. Schmal, Appl. Catal. A Gen. 255 (2003) 83.
[48] M. Aryafar, F. Zaera, Catal. Lett. 48 (1997) 173.
[49] Y.-F. Yao, Ind. Eng. Chem. Prod. Res. Dev. 19 (1980) 293.
[50] V.A. Drozdov, P.G. Tsyrulnikov, V.V. Popovskii, N.N. Bulgakov, E.M. Moroz, T.G. Galeev, React. Kinet. Catal. Lett. 27 (1985) 425.
[51] S. Wang, G.Q. Lu, Energy Fuels 10 (1996) 896.
[52] D.A. Hickman, L.D. Schmidt, Science 259 (1993) 343.
[53] F. Besenbacher, I. Chorkendorff, B.S. Clausen, B. Hammer, A.M. Molenbroek, J.K. Nørskov, I. Stensgaard, Science 279 (1998) 1913.
[54] F.B. Noronha, A. Shamsi, C. Taylor, E.C. Fendley, S. Stagg-Williams, D.E. Resasco, Catal. Lett. 90 (2003) 13.
[55] B. Lang, R.W. Joyner, G.A. Somorjai, Surf. Sci. 30 (1972) 454.
[56] P. Gambardella, Ž. Sljivanĉanin, B. Hammer, M. Blanc, K. Kuhnke, K. Kern, Phys. Rev. Lett. 87 (2001) 056103.
[57] J. Rostrup-Nielsen, J. Nørskov, Top. Catal. 40 (2006) 45.
[58] S. Helveg, C. López-Cartes, J. Sehested, P.L. Hansen, B.S. Clausen, J.R. Rostrup- Nielsen, F. Abild-Pedersen, J.K. Nørskov, Nature 427 (2004) 426.
[59] R.E. Reitmeier, K. Atwood, H.A. Bennet Jr., H.M. Baugh, Ind. Eng. Chem. 49 (1948) 620.
[60] V.R. Choudhary, A.M. Rajput, B. Prabhakar, Catal. Lett. 32 (1995) 391.
[61] J.M. Parera, N.S. Figoli, E.M. Traffano, J.N. Beltramini, E.E. Martinelli, Appl. Catal. 5 (1983) 33.
[62] H.-Y. Wang, C.-T. Au, Catal. Lett. 38 (1996) 77.
[63] S. Tang, J. Lin, K.L. Tan, Catal. Lett. 55 (1998) 83.
[64] K.D. Gibson, M. Viste, S.J. Sibener, J. Chem. Phys. 125 (2006) 133401.
[65] D. Weng, O. Dewaele, A.M. De Groote, G.F. Froment, J. Catal. 159 (1996) 418.
[66] R. Burch, P.K. Loader, Appl. Catal. A Gen. 122 (1995) 169.
[67] F.B. Passos, E.R. Oliveira, L.V. Mattos, F.B. Noronha, Catal. Lett. 110 (2006) 261.